Use of Strain Gages to Predict Soil-Geotextile Interaction in Pullout Tests

Y. Bourdeau, T. Ogunro & P. Lareal
Laboratoire Geotechnique, I.N.S.A., Villeurbanne, France

G. Riondy
B.R.G.M., Pessac, France

ABSTRACT

A method of exploitation of pullout test of a geotextile embedded in a coarse-grained soil is presented. This method based on analytic bond laws leads to a direct determination of the local frictional law of soil-geotextile interface, from only the pullout force-displacement relationship. A good agreement between the calculated local deformations and those measured with strain gages validates this analytical method.

1 INTRODUCTION

The local behavior of a coarse-grained soil-geotextile interface was studied at INSA in Lyon in a large scale pullout tests using Alluvium of Rhône (Alluvions du Rhône) as fill material.

The results presented by Bourdeau et al (1989 and 1990) showed that the pullout force T_A versus the displacement U_A exhibits a peak softenning to a lower residual value (figure 1), irrespective of geotextile's length, overburden and pullout rate.

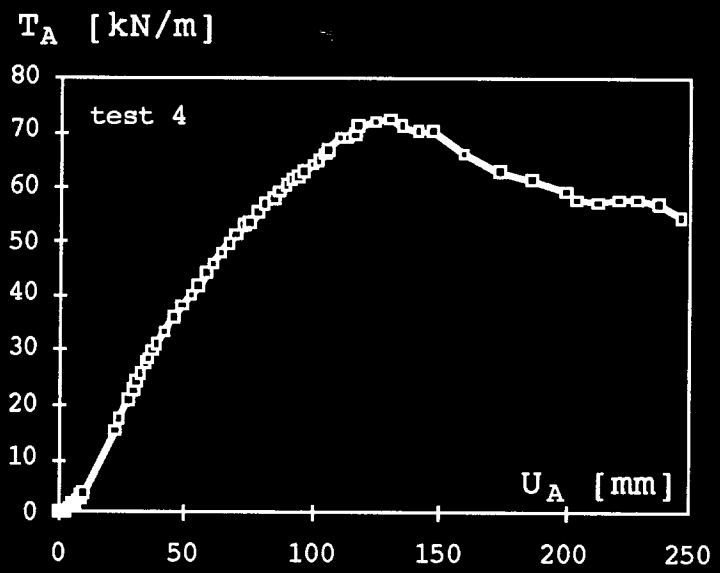

Figure 1 T_A - U_A relationship (L = 2 m)

Using a large shear box of 0.6 m x 0.6 m Bourdeau and Lareal (1989) showed that this softenning phenomenon was also a characteristic of the shear behavior of the alluvium.

Inextensible flexible cables attached to the geotextile enabled us to monitor the evolution of the local displacements U(x) and the progressive mobilisation of the reinforcing geotextile inside the soil mass (figure 2).

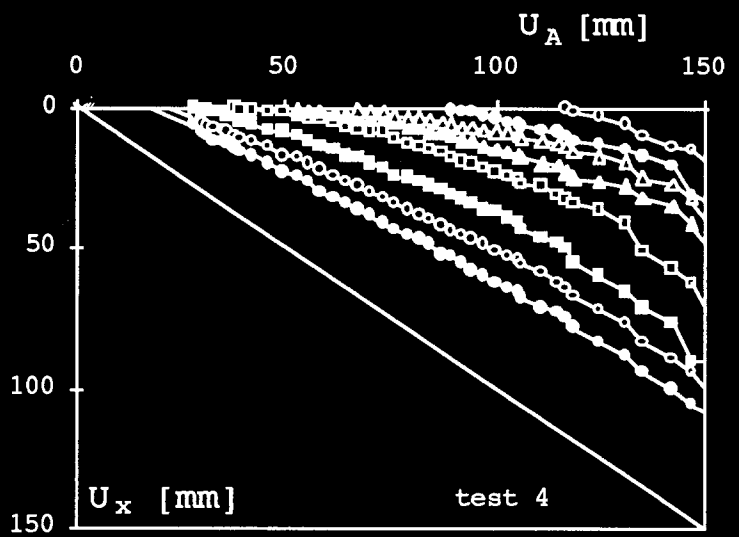

Figure 2 Ux - U_A relationship (L = 2 m)

A pullout displacement of about 5% elongation is generally required to cause movement of the geotextile embedded end.

The finite difference modellings presented by Bourdeau and Kastner (1989) are based on two fundamental assumptions:

- For small deformations the elongation modulus J is very progressive (figure 3, section a), and the extensive behavior of the geotextile can therefore be

approximated by equation (1) corresponding to the linear section (b).
The material behavior represented by initial local strain ε_o enables us to simulate the deformations for which the geotextile is put in tension.

$$\varepsilon(x) = \frac{dU(x)}{dx} = \varepsilon_o + \frac{T(x)}{J} \qquad (1)$$

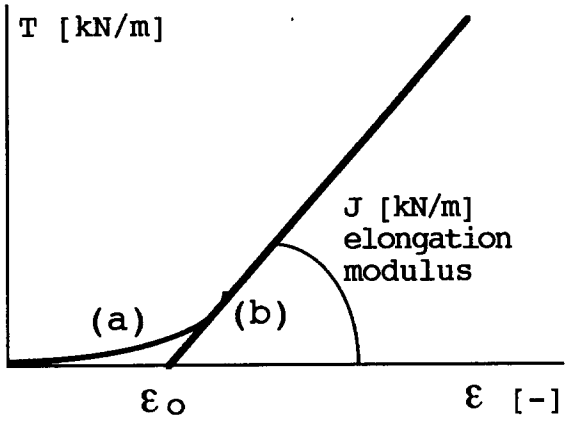

Figure 3 geotextile tensile force-strain relationship

- The soil-geotextile local interfacial frictional relationship takes into account a progressive softenning leading to a residual value τ_r for a displacement superior to the limit displacement U^*. U^* corresponds to the displacement at which maximum frictional stress τ^* is mobilised (figure 4).

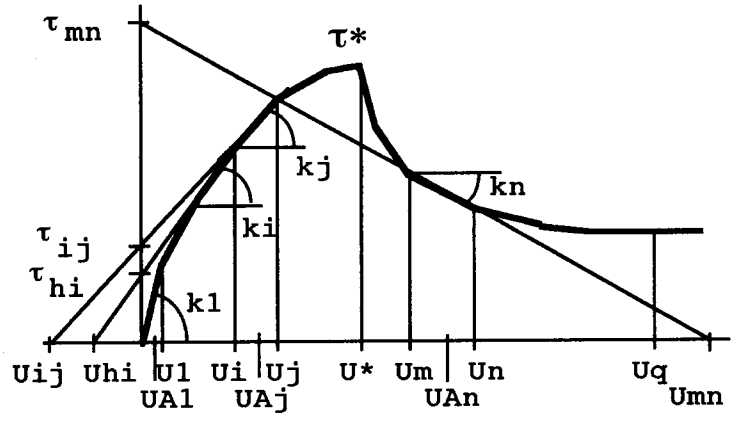

Figure 4 governing local interfacial relationship τ - U

Based on these assumptions, this paper presents an analytic approach of modelling pullout tests. This method proposes a system of exploitation of tests based on the measurements of the total pullout force and displacements of both ends of the geotextile.
It also enables the determination of the soil-geotextile local interfacial frictional behavior and of the value of ε_o introduced in the analysis.

Comparison of the analytical estimation of the local strains with those measured using the strain gages permits the validation of this method and the postulated assumptions.

2 DESCRIPTION OF TESTS MODELS

2-1 Tests conditions

Tests n° 15 and 17 analysed in this paper were performed using geotextile specimens of 1.5 m long by 0.5 m wide (figure 5).
Test 15 was carried out on a geotextile embedded at a depth of 1.95 m in a pullout box of 3 m long by 1m wide by 2.5 m deep.
In order to reduce boundary effects on results, test 17 was performed on a geotextile placed at a depth of 1.05 m inside a large cylindrical container of 3 m diameter by 1.6 m deep.

The geotextile is clamped between two iron plates extending 0.75 m inside the pullout test container. A hydraulic ram of 200 kN transmits a constant pullout rate, in this case 0.1 mm/mn.
The pullout force T_A and the displacement U_A of the clamped end of geotextile were recorded.

The geotextiles were equiped with strain gages with clamping ends 0.15 m apart manufactured by BRGM. For their bulky sides (i;e the Strain Gages), each geotextile was equiped with only two gages, one near the clamped end and the other towards the embedded end.
For the tests presented in this paper the gages were located close to the clamped end at average distances of 0.375 m and 0.325 m respectively (figure 5).
In addition two flexible inextensible cables were also fixed on either sides of the gages to measure the evolution of the local displacements and hence to establish sources of comparison with the strain gages' measurements.

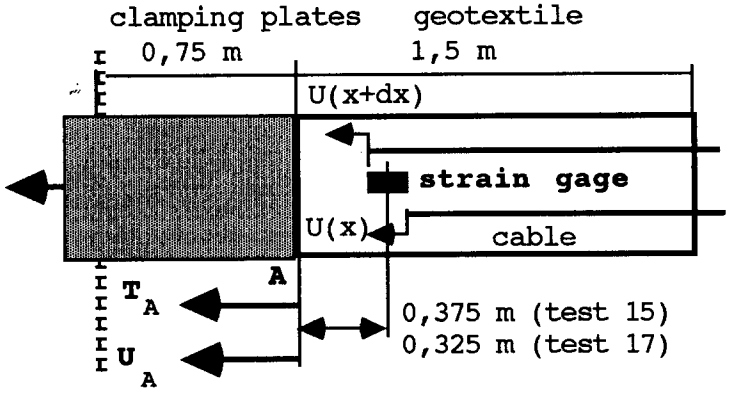

Figure 5 geotextile instrumentation

2-2 Materials characteristics

The part of the alluvium of Rhone passing through a sieve of size 32 mm was used as the tested soil in order to avoid local puncture and tearing of the geotextile observed in some earlier tests. The soil was placed at an apparent unit weight of about 20 KN/m^3.
The internal angle of friction ϕ measured using a large shear box of 0.6 m by 0.6 m is 35°.

The reinforcement is a woven- knitted geotextile (polyester) having an elongation modulus J = 1100 kN/m and ultimate tensile strength of 150 kN/m.

3 ANALYTIC MODELLING

3-1 Hypothesis

We consider the general case of a local interfacial frictional behavior exhibiting a marked peak that leads to a lower limiting value, approximated by successive linear sections (figure 4).

Assuming that the geotextile is sufficiently flexible so that its embedded end B only moved for a displacement superior to the limit displacement U*, corresponding bond laws can be written for the 4 phases of the phenomenological study of pullout test as in figure 6.

The first three phases (denoted 1, j, n) describe the evolution of the mobilized force T_A as the geotextile is put under progressive tension, while the fourth phase (denoted q) shows the effect of the embedded end's displacement U_B on the analysis.

This analysis can be expanded to include other forms of reinforcements one of which is a rigid inclusion for which interface bond is rapidly mobilized and which can lead to the movement of the embedded end for a displacement inferior to the limit displacement.

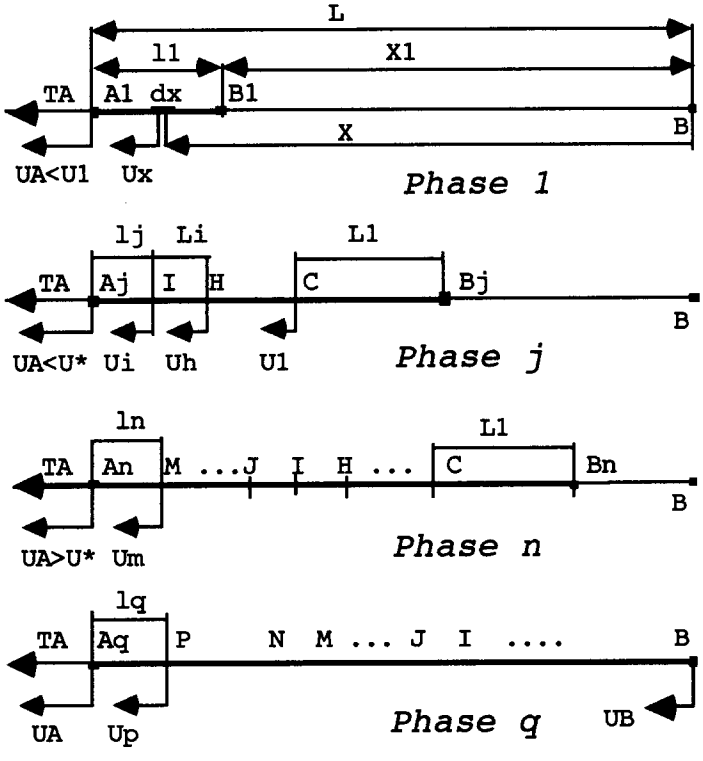

Figure 6 evolution of geotextile mobilization

3-2 Phase 1:

U_A (position A_1) < U_1 as figures 4 and 6

The frictional force along an elementary length dx is given by (2).

$$dT = 2\,\tau\,dx \qquad (2)$$

where $\tau = k_1 U$ (3)

Resolving equations (1) to (3), Bourdeau and al (1991) arrived at expression (4) for the total pullout force.

$$T_{A1} = J\,\varepsilon_o\,[ch(\beta_1 l_1) - 1] \qquad (4)$$

Length l_1 of the section A_1B_1 is defined by (5).

$$sh(\beta_1 l_1) = \frac{\beta_1\,U_{A1}}{\varepsilon_o} \qquad (5)$$

l_1 attains the optimum value L_1 once $U_{A1} = U_1$. This optimum length L_1 obeying relationship (3) will be conserved towards the rear end of the reinforcement as long as the embedded end of the geotextile does not move ($U_B = 0$).

Combining expressions (4) and (5) gives the non-dimensionnal expression (6).

$$[A_1] = \frac{T_{A1}}{J} + \varepsilon_o = \sqrt{\varepsilon_o^2 + (\beta_1\,U_{A1})^2} \qquad (6)$$

3-3 Phase j:

$U_i < U_A$ (position A_j) $< U_j$ as figures 4 and 6

$U_j < U^*$ and U_B (position B_j) = 0

The local friction mobilized by section A_jI (at the clamped end) of lenghth l_j obeys the relationship:

$$\tau = \tau_{ij} + k_j\,U(x)$$

which leads to the differential equation:

$$\frac{d^2U(x)}{dx^2} - \beta_j^2\,U(x) = \frac{2\,\tau_{ij}}{J}$$

with $\beta_j = \sqrt{\frac{2\,k_j}{J}}$

The general solution becomes:

$$U(x) = U_{ij} + C_1\,e^{\beta_j x} + C_2\,e^{-\beta_j x}$$

$$T(x) = \beta_j\,J\,(C_1\,e^{\beta_j x} - C_2\,e^{-\beta_j x}) - \varepsilon_o\,J$$

where $U_{ij} = -\frac{\tau_{ij}}{k_j}$ (figure 4)

Resolving and rearranging the system of equations lead to the non-dimensional equation (7).

$$[A_j]^2 = [I]^2 + \beta_j^2\,[(U_{Aj} - U_{ij})^2 - (U_i - U_{ij})^2] \qquad (7)$$

with $[Aj] = \frac{T_{Aj}}{J} + \varepsilon_o$

and $[I] = \frac{T_I}{J} + \varepsilon_o$

T_{Aj} and T_I are respectively the total pullout force and the force at point I.

The length l_j of section A_jI is given by the expression:

$$e^{\beta_j l_j} = \frac{[A_j] + \beta_j\,(U_{Aj} - U_{ij})}{[I] + \beta_j\,(U_i - U_{ij})}$$

The same analysis is applied to the following sections (or elements):
IH, ..., CB_j.

3-4 Phase n:

$U_m < U_A$ (position A_n) $< U_n$ as figures 4 and 6

$Um > U^*$ and U_B (position B_n) = 0

The mobilized friction on the extreme position A_nM of length l_n is governed by:

$$\tau = \tau_{mn} - k_n U(x)$$

Similar to the procedure adopted for phase (j), we have the non-dimensionnal expression (8) below.

$$[A_n]^2 = [M]^2 - \beta_n^2 [(U_{An} - U_{mn})^2 - (U_m - U_{mn})^2] \quad (8)$$

in which $\beta_n = \sqrt{\frac{2\ k_n}{J}}$

and $U_{mn} = \frac{\tau_{mn}}{k_n}$ (figure 4)

with $[An] = \frac{T_{An}}{J} + \varepsilon_o$

and $[M] = \frac{T_M}{J} + \varepsilon_o$

where T_{An} and T_M represent the total pullout force and the force at point M.
The length l_n of section A_nM is given by:

$$\tan(\beta_n l_n) = \frac{\frac{[A_n]}{\beta_n (U_{mn} - U_{An})} - \frac{[M]}{\beta_n (U_{mn} - U_m)}}{1 + \frac{[A_n]\,[M]}{\beta_n^2 (U_{mn} - U_{An})(U_{mn} - U_m)}}$$

These relationships apply to all sections towards the clamped end satisfying local displacement greater than the limit displacement U^*. Towards the embedded end, all sections having local displacements inferior to U^* are governed by the given relationships of phase (j).

Note that the equations (6) to (8) for the phases described above can be represented by $T_A = f(U_A)$ and differenciating gives the general expression (9).

$$\left(\frac{dT_A}{dU_A}\right) = \frac{2\,\tau_A}{[A]} \quad (9)$$

where τ_A is the friction mobilized at the clamped end.

3-5 Phase q:

$U_B > 0$ and $\tau_B > 0$ as figure 6

The preceeding relashionships remain valid except for the section at the embedded end which progressively develops towards zones (j), (n) ...

The mobilized friction at B will successively become (10):

$$\tau_B = k_1 U_B \ldots = k_j (U_B - U_{ij}) \ldots = k_n (U_{mn} - U_B) \quad (10)$$

For a non-zero displacement of the embedded end of the geotextile, the differenciation of the relationship $T_{Aq} = f(U_{Aq})$ becomes (11):

$$\left(\frac{dT_A}{dU_A}\right) = \frac{2\,\tau_{Aq} - 2\,\tau_B \left(\frac{dU_B}{dU_A}\right)}{[A_q]} \quad (11)$$

4 EXPLOITATION OF PULLOUT TEST

4-1 Initial strain ε_o determination

Bourdeau et al (1991) presented a graphical method of determination of initial ε_o based on the assumption that the local frictional law is linear for small displacements. The beginning part of the experimental T_A-U_A relashionship corresponds to phase (1) described above.
Transformation of equation (6) gives a linear relashionship (12) in terms of T_A/J and U_A^2/T_A.

$$\frac{T_{A1}}{J} + 2\,\varepsilon_o = 2\,k_1 \frac{U_{A1}^2}{T_{A1}} \quad (12)$$

The result of the application of this method on test 17 is given in figure 7. Its intersection with the ordinate gives the value of ε_o as 1,42%.
The application on test 15 (not shown here) gives the value of ε_o as 1,90%.
Determination of the initial gradient (modulus k_1) and displacement U_1 (corresponding to the point of gradient's change) from figure 7 enables the verification of method proposed in paragraph 4.2.

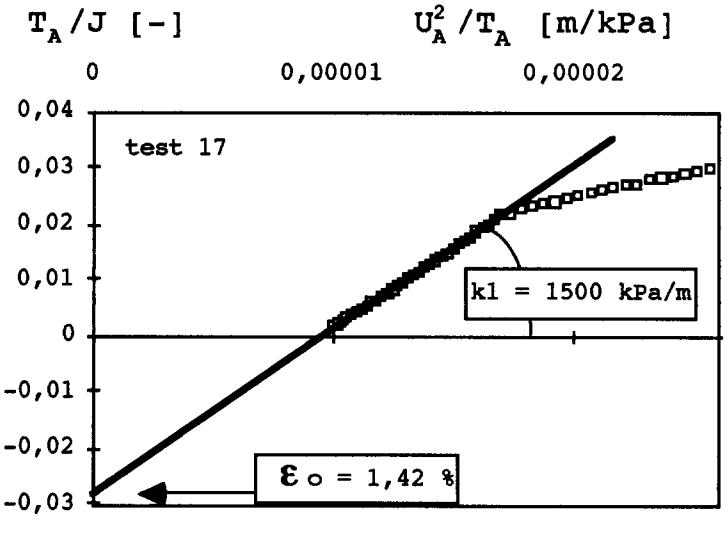

Figure 7 determination of ε_o (test 17)

4-2 Local interfacial frictional relationship determination

Utilizing expressions (7) and (8), a step by step method similar to paragraph 4.1 enables the determination of the governing local frictional relationship $\tau = f(U)$.

A more direct method of determining this law from a general expression (13), developed from (11), it permits expressing the friction at the clamped end τ_A on function of the gradient of the T_A-U_A and U_B-U_A relationships.

$$\tau_A = \frac{1}{2}\left(\frac{T_A}{J} + \varepsilon_o\right)\left(\frac{dT_A}{dU_A}\right) + \tau_B \left(\frac{dU_B}{dU_A}\right) \quad (13)$$

The second term remains zero as long as the embedded end does not move (verifying equation (9) for phases 1, j, n).
This procedure should therefore be carried out in two stages, the first part of the law determined before the movement of the embedded end permits the evaluation of τ_B (from (10)) to be used in (13).
To avoid too much dispersal of data points, this approach requires a prior smoothing of the T_A-U_A and U_B-U_A relationships.

Figure 8 presents the result of this method of exploitation on test 17 (geotextile: J = 1100 kN/m and ε_o = 1,42%).
An abrupt softenning of the local friction τ is noticed immediatly the local displacement U^*. Examining figure 9 (T_A-U_A relationship) shows that this softening phenomenon continues as long as the maximum force (resistance) is not attained.

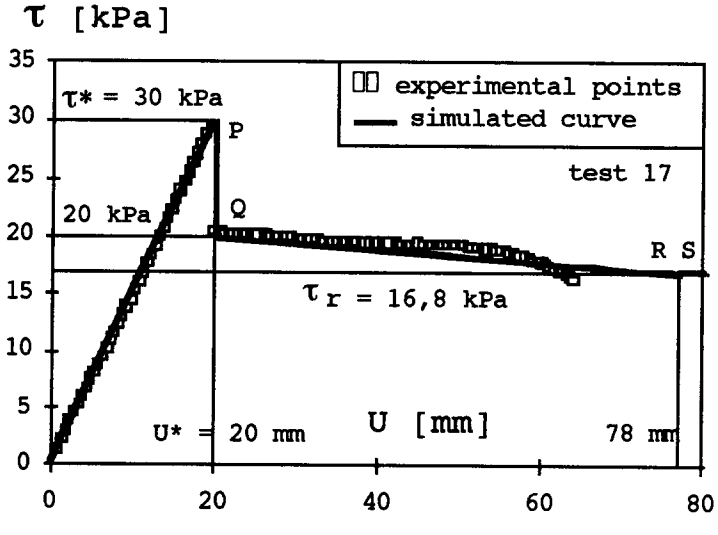

Figure 8 local interfacial frictional relationship (test 17)

4-3 Analytic modelling of the T_A-U_A relationship

Assuming on one hand that the local frictional law can be approximated by 4 successive linear elements (figure 8, path OPQRS), and on the other hand that the residual friction τ_r is attained at the instant when the pullout force is maximum, the pullout force - displacement relationship can then be modelled using the analytic expressions developed earlier.
Figure (9) shows the good agreement between the calculated curve and the experimental values.

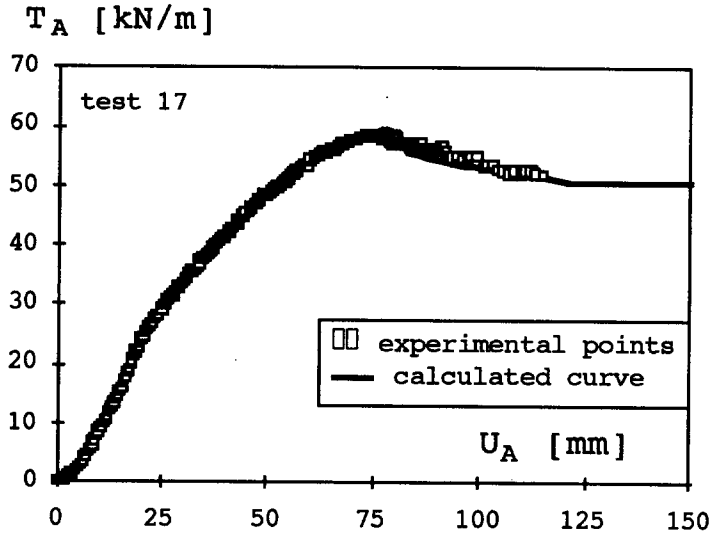

Figure 9 comparison of T_A-U_A curves (test 17)

4-4 Analytic modelling of local deformations

The method described in 4.3 can be extended to evaluate local deformations $\varepsilon(x)$.
Figures 10 (test 15) and 11 (test 17), representing the evolution of the local deformations with pullout displacements, shows a relatively satisfactory agreement between calculated values and experimental points. The rupture notwithstanding of the gage's cable in the course of test 17 at a displacement of 55 mm.
The deformation estimated from the measured local displacements U(x) carried out on either sides of the gage (figure 5) enables us however to compensate for the disruption of the gage measurement for test 17.

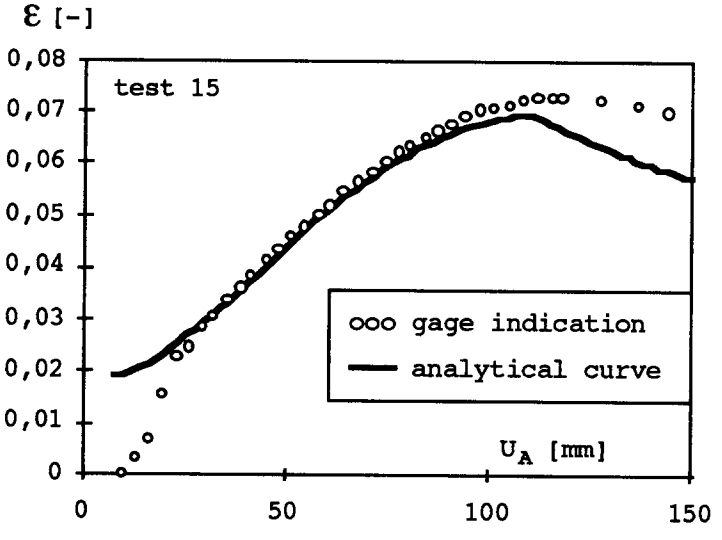

Figure 10 comparaison of ε-U_A relationship (test 15)

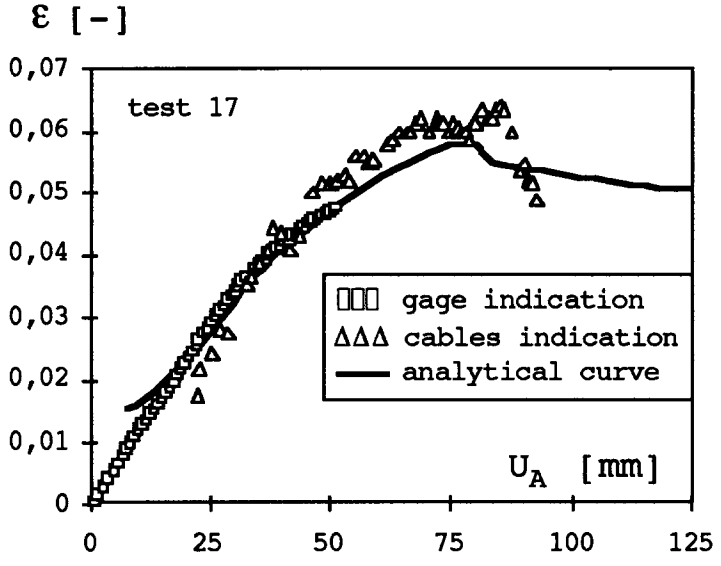

Figure 11 comparaison of ε-U_A relationship (test 17)

The slight disparity between the values of the calculated and the measured strains at the biginning of the tests can be traced to the simplified relationship of the tensile law (figure 3, section b) used in the analysis. However, taking into consideration of the progressive elongation modulus (figure 3, section a) should reduce this difference.
The difference beyond the peak can be explained by the presence of the gage rendering the normal contraction of the geotextile impossible in the softening phase.

It is also noticed that the gage's reaction requires a signifiant pullout displacement more important in test 15 than in test 17, confirming the progressive put on tension of the geotextile.

4-5 Estimation of soil-geotextile friction angle

The coefficient of apparent limit friction μ^* at the soil-geotextile contact can be determined from the value of the limit friction τ^* of the local frictional law (figures 4 and 8), or even a coefficient of average apparent friction μ_m and a friction angle ϕ_m from the maximum pullout force (figure 9).
These values are determined assuming that the normal stress σ corresponds to the weight of the overburden soil (table 1).

tableau 1 friction-coefficient and soil-géotextile friction angle

	Essai 15	Essai 17
σ (kPa)	39	21
τ^* (kPa)	27,6	30
$\mu^* = \tau^* / \sigma$	0,708	1,428
τ_m (kPa)	21,7	20
$\mu_m = \tau_m / \sigma$	0,556	0,952
ϕ_m	29°1	43°6

It is noticed that the values of test 15 performed in a large box of 1 m wide are considerably smaller than those of test 17 carried out in a large cylindrical container of 3 m diameter.
Even though the reduction of the friction can partly be attribued to boundary effects, it is due essentially according to Boulon et al (1991) to the phenomenon whereby the friction descreased with increased overburden soil and/or with decreased normal stiffness.
The values of ϕ_m can be compared to the friction angle of soil $\phi = 35°$.

5 CONCLUSION

The results of the proposed analytic method used in this publication compare well with the experimental measurements. Even if boundary effects affect the measurements to some extend, the obtained results coupled with the observed phenomena justify the used of large scale tests for the study of the bond behavior of the pullout of a geotextile placed in a coarse - grained soil.

REFERENCES

Bourdeau Y., Laréal P., Bahloul F. "Comportement à l'extraction de nappes géosynthétiques de grandes dimensions". Séminaire National du GRECO "Rhéologie des Géomatériaux", rapport scientifique 1988, pp. 294-298, Aussois, Décembre 1988.

Bourdeau Y., Laréal P., Marchal J. "Résistance au cisaillement des alluvions du Rhône". C.R. 12° International Conference on Soil Mechanic and Foundation Engineering, vol. 1, pp. 695-696, Rio de Janeiro, Août 1989.

Bourdeau Y., Kastner R. "Etude de l'interaction sol-géotextile par essais d'arrachement". C.R. Journées Franco-Tunisiennes "Mécanique des Sols: Stabilité et Renforcement des Pentes", pp. 39-45, Paris, Mai 1989.

Bourdeau Y., Kastner R. "Comportement en extraction d'une inclusion déformable. Détermination de la loi de cisaillement à l'interface". C.R. 3° Entretiens du Centre Jacques Cartier "Méthodes Numériques en Mécanique des Sols, application aux Renforcements des Sols et des Roches", 22 pp., Grenoble, Décembre 1989.

Bourdeau Y., Kastner R., Bollo-Kamara N., Bahloul F. "Comportement en ancrage d'un géosynthétique enfoui dans un matériau bidimensionnel". Archive of Hydro-technics, vol. XXXVIII, n° 1-2, pp. 117-130, 1991.

Boulon M., Bourdeau Y., Delage P., Edil T.B. "Frottement sol-inclusion dans les sables: aspects expérimentaux et interprétation". Séminaire National du GRECO "Rhéologie des Géomatériaux", rapport scientifique 1991, pp. 343-355, Aussois, Nov. 1991.

Bourdeau Y., Riondy G., Colin J.C. "Utilisation de jauges de déformation pour l'étude du comportement en ancrage d'une nappe géotextile noyée dans un matériau grossier". Séminaire National du GRECO "Rhéologie des Géomatériaux", rapport scientifique 1992, pp. 303-309, Aussois, Novembre 1992.